

# A Monolithically 3-D Printed Waveguide Filter Based on Elliptic Cylindrical Resonators With Enhanced Polarization Rotation Flexibility

Yuhong Ye<sup>#\$\*1</sup>, Jin Li<sup>#\$\*2</sup>, Sicheng Chen<sup>#\$\*</sup>, Zhihong Xu<sup>#\$\*</sup>, Tao Yuan<sup>#\$\*</sup>

<sup>#</sup>Guangdong Provincial Mobile Terminal Microwave and Millimeter-Wave Antenna Engineering Research Center, College of Electronics and Information Engineering, Shenzhen University, China

<sup>\$</sup>Guangdong-Hong Kong Joint Laboratory for Big Data Imaging and Communication, China

<sup>\*</sup>State Key Laboratory of Millimeter Waves, China

<sup>1</sup>yeyuhong2021@email.szu.edu.cn, <sup>2</sup>jinli.cie@szu.edu.cn

**Abstract**— This paper reports on a new class of waveguide filter with enhanced flexibility in the realization of polarization rotation functionality. The filter is based on elliptic cylindrical resonators (ECRs) that are configured with an in-line coupling topology using cylindrical coupling cavities. The polarization rotation functionality of the filter is enabled by rotating the ECRs along the axis of symmetry with appropriate angle intervals. Any polarization rotation angle between 0°–90° can be readily achieved without any distortion of the filter geometry. An X-band fourth-order filter prototype with a polarization rotation angle of 90° and a Chebyshev bandpass transfer function is designed and implemented. The filter is manufactured monolithically by incorporating Polyjet 3-D printing and electroless copper plating techniques. The 3-D printed filter demonstrates excellent RF performance with passband return loss and insertion loss of over 20 dB and averagely 0.4 dB, respectively.

**Keywords**— bandpass filter, elliptic cylindrical resonator, monolithic prototyping, polarization rotation, Polyjet 3-D printing, waveguide filter.

## I. INTRODUCTION

Microwave waveguide filters capable of realizing twisted transmission paths and rotated polarization orientations for versatile conformal communication systems have been of great interest to the filter research community. Innovation of these filters is attributed to the rapid development of additive manufacturing technology that successfully deals with the complex twisted and rotated filter geometries. Conventional twisted or polarization-rotated waveguide filters are composed of in-series cascaded filters and twists that are designed and manufactured individually [1]–[5]. This is at expense of redundant size and large RF loss of the filter. In recent years, the waveguide twist has been integrated into the filter geometry and typical filters of this type have been implemented with 3-D printing techniques such as stereolithography apparatus (SLA) and selective laser melting (SLM) [6]–[9].

In previous work, these 3-D printed filters are constructed by directly bending and twisting the rectangular waveguide (RWG) or step-rotating the RWG resonators. The twisted RWG iris filter reported in [6] has relatively large longitudinal size. An alternative with a reduced length of the filter is composed of step-rotated RWG resonators [7]. Other filters with direct bending and twisting in 90° of the RWG are presented in [8] and [9]. These filters suffer undesired distortion of the twisted waveguide cavities that can be hardly modeled in the

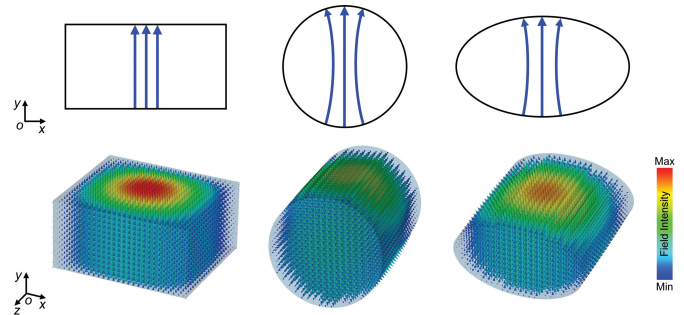


Fig. 1. Simulated electric field distribution of the dominant mode in rectangular (left: TE<sub>10</sub> mode), cylindrical (middle: TE<sub>11</sub> mode), and elliptical (right: TE<sub>e11</sub> mode) waveguides. The blue arrows in the cross-sectional views indicate the electric field orientation of the dominant mode.

electromagnetic (EM) simulation. In addition, the distorted cavity geometries exhibit poor compatibility with 3-D printing process. For example, 3-D printing the twisted RWG iris filter would use supporting structures inside the waveguide and the 3-D printed irises could be deformed or damaged due to several aspects including insufficient mechanical strength, residual stress in the printing material, and surface processing of the 3-D printed parts. This makes RF performance of the filter highly dependent on the post fabrication process of 3-D printing and it dramatically increases uncertainty in the quality control of the filter.

In this work, a new class of 3-D-printing-compatible polarization-rotated waveguide filter architecture is proposed to address the aforementioned issues. An X-band fourth-order waveguide bandpass filter (BPF) based on elliptic cylindrical resonators (ECRs) and with a polarization rotation angle of 90° is demonstrated as proof of concept. The filter design incorporates the fundamental principle of additive manufacturing and takes advantages of rotational symmetry of the ECRs and cylindrical coupling cavities. The filter features flexible design of any polarization rotation angle between 0°–90° without distortion of the cavity geometry. Design, manufacture, and RF measurement of the proposed filter are described in the following content of this paper.

## II. FILTER DESIGN

It is straightforward to understand that cavity geometries in rotational symmetry are the most appropriate candidates

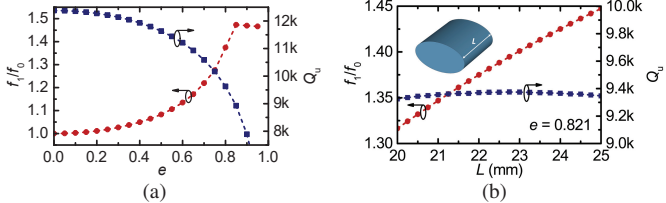


Fig. 2. EM simulation to determine cross-sectional and longitudinal dimensions of the ECR. (a) The simulated  $f_1/f_0$  and  $Q_u$  under different  $e$  values. The fundamental-mode frequency is kept at 10 GHz. (b) The simulated  $f_1/f_0$  and  $Q_u$  under different lengths of the resonator.

for the filter because the resonator and coupling structures would be independent of the polarization rotation angle. A typical geometry satisfying the rotational symmetry is the circular waveguide (CWG) cavity. However, stopband performance of the CWG filter is restricted intrinsically by the degenerate modes and the spurious modes. An alternative with improved distribution of the degenerate and spurious modes is the elliptical waveguide (EWG) cavity. Fig. 1 illustrates simulated electric field distribution of the dominant mode in the aforementioned three types of waveguides. It shows strong similarity in the field distribution, and particularly, the field components of these modes are mostly in parallel with each other in the  $xoy$  plane. Therefore, it is reasonable to build a polarization-rotated filter with combination of CWG and EWG cavities. In this work, elliptic cylindrical and regular cylindrical cavities are exploited as resonators and coupling structures, respectively.

In the first step of the filter design, a proper geometry of the ECR is selected taking into account the frequency ratio of the first higher-order mode to the fundamental mode ( $f_1/f_0$ ) and the unloaded quality factor ( $Q_u$ ). Fig. 2(a) depicts simulated  $f_1/f_0$  and  $Q_u$  values of the ECR with different eccentricities ( $e$ ) of the elliptic cross-sectional contour. It shows that increasing  $e$ , i.e., a flatter ECR, results in a larger  $f_1/f_0$  ratio and a dramatically reduced  $Q_u$ . For  $e = 0$ , the  $f_1$  and  $f_0$  represent frequencies of the two orthogonal degenerate modes in a CWG. They are no longer identical in the ECR ( $0 < e < 1$ ) due to splitting of the degenerate modes. The  $Q_u$  of a flatter ECR is much lower because of the highly reduced cavity volume. In spite of the maximum achievable  $f_1/f_0$  ratio of 1.473 for  $e = 0.85$ , an  $e$  value of 0.821 is selected to balance the  $Q_u$ . The  $Q_u$  values are evaluated using copper boundaries with an electrical conductivity ( $\sigma$ ) of  $5.96 \times 10^7$  S/m and a root-mean-square surface roughness ( $R_q$ ) of 2  $\mu\text{m}$ . It should be mentioned that the fundamental mode is always  ${}_e\text{TE}_{111}$  with increasing  $e$  whereas the first higher-order mode varies. For example, the first higher-order mode is  ${}_e\text{TM}_{010}$  for  $e = 0.6$  and it turns into  ${}_e\text{TE}_{112}$  for  $e = 0.84$ . Fig. 2(b) presents the simulated  $f_1/f_0$  and  $Q_u$  values of the ECR ( $e = 0.821$ ) with different cavity lengths and the corresponding frequency  $f_0$  range is 9.84–10.82 GHz. It shows that elongation of the ECR results in a reduced  $f_0$ , a small increase in the  $f_1/f_0$  ratio, and little variation in the  $Q_u$ .

The inter-resonator coupling of the filter is realized by a cylindrical cavity between two adjacent ECRs and the external

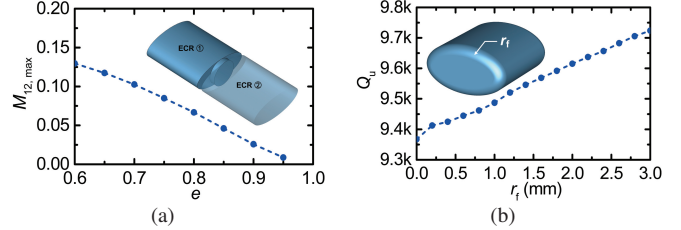


Fig. 3. EM simulation and geometrical optimization of the ECR. The fundamental-mode frequency is kept at 10 GHz. (a) The simulated  $M_{12,\max}$  under different  $e$  values. (b) The simulated  $Q_u$  under different  $r_f$  values.

coupling is achieved by a cylindrical cavity between the RWG port and the adjacent ECR. The coupling strength is controlled by both size of the cylinder and the rotation angle of the ECRs. The coupling is weakened with the increase in the rotation angle because of the reduced amount of parallel electric field components from the coupled modes. Particularly, the coupling is eliminated as the rotation angle reaches the maximum of  $90^\circ$ . Decreasing size of the cylinder weakens the coupling as well. The maximum inter-resonator coupling strength is reached with a rotation angle of  $0^\circ$  and a diameter of the cylinder equal to the length of the minor axis of the ellipse. Fig. 3(a) shows the maximum achievable inter-resonator coupling coefficient  $M_{12,\max}$  that is extracted using the approach outlined in [10] for the two coupled ECRs. The  $M_{12,\max}$  for  $e = 0.821$  is about 0.06 and the practical coupling coefficients associated with the filter design specifications need to be smaller than this value. It is known from Fig. 3(a) that the maximum achievable bandwidth of the filter is also related to  $e$ , i.e., the geometry of the ellipse. Therefore, the bandwidth requirement of the filter needs to be considered to finalize the ECR structure. Edges of the ECR are filleted to improve the structural compatibility with 3-D printing process [11], [12] and the fillets slightly improve  $Q_u$  of the ECR. Fig. 3(b) shows the simulated  $Q_u$  values with increasing the fillet radius  $r_f$ . The  $r_f$  value can be selected flexibly regardless of other geometrical parameters because the fillets do not compromise the rotational symmetry or the coupling strength.

A fourth-order BPF prototype with an overall polarization rotation angle of  $90^\circ$  is designed at X band. EM simulation and parameter optimization of the BPF are performed in CST Studio Suite [13]. The air-cavity and package models of the filter are illustrated in Figs. 4(a) and 4(b), respectively. The filter comprising the filleted ECRs and the cylindrical cavities is configured with an in-line coupling topology and the ECRs are rotated in increasing angles with a constant interval  $\Delta\alpha$  of  $18^\circ$ . The angle interval  $\Delta\alpha$  is determined by the five rotated stages including the ECRs and the waveguide ports. It can be selected flexibly depending on the overall polarization rotation angle and the number of rotated stages. More rotated stages produce a smaller  $\Delta\alpha$  but larger filter size. The  $\Delta\alpha$  value can be different for each rotating stage and the difference can be compensated by adjusting size of the corresponding cylindrical coupling cavity. The filter is designed with a Chebyshev bandpass transfer function at a passband center frequency of 10 GHz, a fractional bandwidth

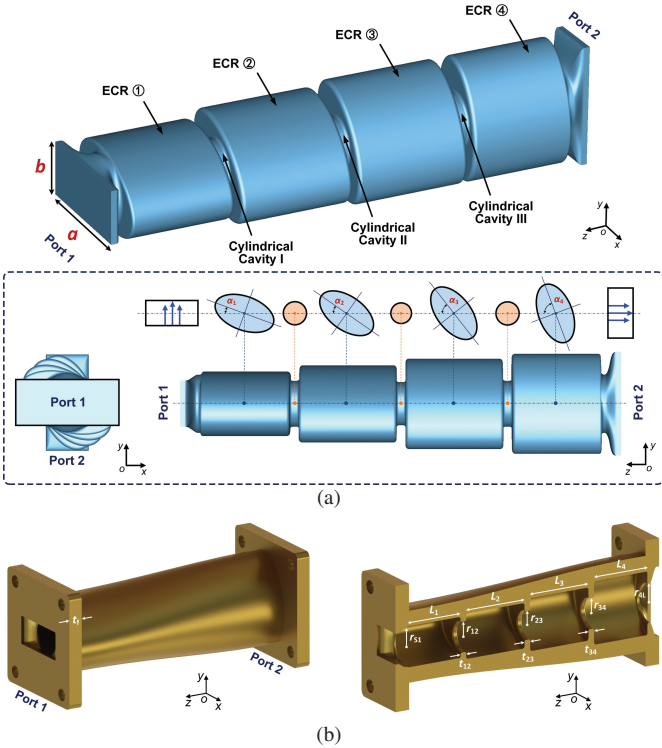


Fig. 4. Physical modeling and EM simulation of the designed X-band polarization-rotated waveguide filter. Critical dimensions of the filter are  $a = 22.86 \text{ mm}$ ,  $b = 10.16 \text{ mm}$ ,  $\alpha_1 = 18^\circ$ ,  $\alpha_2 = 36^\circ$ ,  $\alpha_3 = 54^\circ$ ,  $\alpha_4 = 72^\circ$ ,  $t_f = 5 \text{ mm}$ ,  $r_{S1} = r_{4L} = 6.425 \text{ mm}$ ,  $r_{12} = r_{34} = 5.074 \text{ mm}$ ,  $r_{23} = 4.761 \text{ mm}$ ,  $L_1 = L_4 = 19.642 \text{ mm}$ ,  $L_2 = L_3 = 21.498 \text{ mm}$ ,  $t_{12} = t_{34} = 2 \text{ mm}$ , and  $t_{23} = 2 \text{ mm}$ . (a) The air-cavity simulation model in 3-D and lateral views. The insets illustrate cross-sectional contours of the ECRs and the cylindrical coupling cavities. The blue arrows at the input and output RWG ports indicate the TE<sub>10</sub>-mode electric field orientations. (b) The package model in 3-D and half cutaway views.

(FBW) of 3%, and a passband return loss (RL) of 21 dB. A coupling-matrix-based filter design methodology detailed in [10] is utilized and the non-zero coupling matrix entries are  $M_{S1} = M_{4L} = 0.0318$ ,  $M_{12} = M_{34} = 0.0280$ , and  $M_{23} = 0.0214$ . The corresponding external quality factor ( $Q_e$ ) is 29.7. The desired  $Q_e$  and inter-resonator coupling coefficients  $M_{12}$  and  $M_{23}$  are acquired from the EM-simulated result in Fig. 5(a), where dimensions of the cylindrical cavities are initialized for both external and inter-resonator couplings. Fig. 5(b) exemplifies the reducing  $M_{12}$  and  $M_{23}$  with increasing  $\Delta\alpha$  and the result has proved enhanced design flexibility in the filter's coupling structure.

Note that ECRs of the filter can be rotated in a counterclockwise orientation along the  $-oz$  axis that is opposite to the one illustrated in Fig. 4 and the rotation in neither orientation would distort the filter geometry. Internal edges of all the cavities are filleted to form smooth surface that is highly compatible with 3-D printing process. The EM-simulated result of the filter shows a desired bandpass frequency response with the first spurious passband appearing at around 14 GHz.

### III. FABRICATION, MEASUREMENT, AND DISCUSSION

The filter was manufactured by incorporating high-precision Polyjet 3-D printing and copper electroless plating pro-

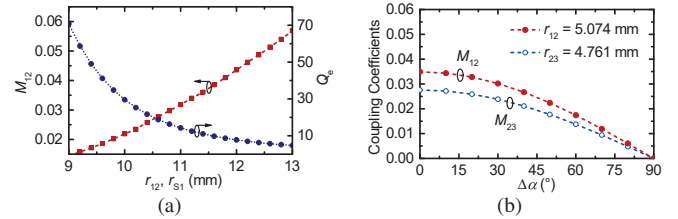


Fig. 5. EM simulation of the two coupled ECRs with optimized geometries. (a) The simulated  $M_{12}$  and  $Q_e$  under different radii of the cylindrical coupling window. (b) The simulated  $M_{12}$  and  $M_{23}$  under different  $\Delta\alpha$  values.

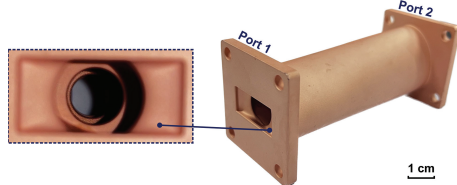


Fig. 6. Photographs of the manufactured X-band polarization-rotated waveguide filter. The inset provides a close-up view of the 3-D printed and copper-plated coupling irises.

cesses. The package model illustrated in Fig. 4(b) was placed vertically for 3-D printing and the Polyjet process was carried out along the  $+oz$  axis in a printing resolution of 20  $\mu\text{m}$ . 3-D printing along this orientation allowed inner sidewalls of the filter to be constructed with minimized surface roughness and it resulted in suspended coupling irises that could be formed by filling the cavities with supporting structures. The model was Polyjet-printed monolithically with a low-density and heat-resistant photosensitive resin and the support was Polyjet-printed simultaneously with a low-melting-point photosensitive wax. The 3-D printed model was hard baked in a blast drying oven to further cure the resin as well as remove the wax support. The cured resin was capable of handling a temperature as high as 120 °C and the wax was melted at around 40 °C. Therefore, it was rather easy to remove all the support by baking. The model was then cleaned and electroless plated with a 10- $\mu\text{m}$  thick layer of copper. Photographs of the manufactured filter are included in Fig. 6.

RF performance of the filter was measured by using a Keysight N5224A network analyzer under a two-port waveguide thru-reflect-line calibration. The power reflection and transmission responses of the filter were measured at X and Ku bands individually. The simulated and measured reflection and transmission coefficients ( $S_{11}$  and  $S_{21}$ ) are graphically compared in Fig. 7, showing excellent agreement that successfully validates the polarization rotation functionality of the filter. The measured passband RL is greater than 20 dB and the corresponding passband insertion loss (IL) is averagely 0.4 dB. The measured frequency shift  $\Delta f$  is as low as 0.2% (~20 MHz) toward higher frequencies, indicating small tolerance and high reliability of the utilized fabrication process. The measured group delay of the  $S_{21}$  parameter is mostly lower than 4 ns in the passband and the RF loss ( $1 - |S_{11}|^2 - |S_{21}|^2$ ) is mainly attributed to the conductor loss from copper due to surface roughness. Major technical attributes of the demonstrated filter are summarized in Table 1 in a quantitative comparison with

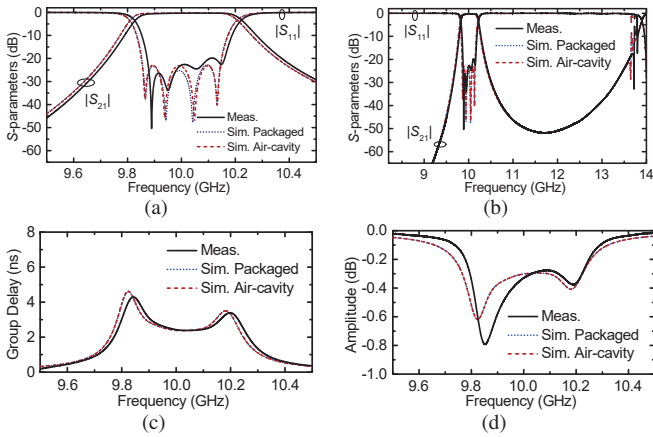


Fig. 7. The EM-simulated and RF-measured results of the filter. Copper boundaries with  $\sigma = 5.96 \times 10^7$  S/m and  $R_q = 2$   $\mu\text{m}$  are used for the simulated result. (a) The passband performance. (b) The wideband performance. (c) The  $S_{21}$  group delay. (d) The loss ( $1 - |S_{11}|^2 - |S_{21}|^2$ ) of the filters.

Table 1. Technical comparison with previously reported polarization-rotated waveguide filters.

Ref.	$f_0$ (GHz)	FBW	IL (dB)	RL (dB)	$\Delta f$	WG Archits.	G.D.?	Process (M.I.?)
[4]	11.8 12.2	2.5% 2.5%	N/A	<sup>a</sup> >18 <sup>a</sup> >20	N/A	RWG	w/o (Medium)	N/A
[6]	33.875	2.9%	0.81	>15	0.37%	RWG	w/ (Poor)	SLA (✓)
[7]	31.9	3.13%	0.84	>15	0.32%	RWG	w/ (Medium)	SLA (✓)
[8]	15	4%	0.85	>13	N/A	RWG	w/ (Poor)	SLA (✓)
<sup>b</sup> [9]	N/A	N/A	<0.2	>20	N/A	RWG	w/ (Poor)	SLM (✓)
T.W.	10.02	3%	0.4	>20	0.2%	EWG	w/o (Good)	Polyjet (✓)

\*T.W.: This work; N/A: Not Available; WG Archits.: Waveguide Architectures; G.D.: Geometrical distortion; D.F.: Design flexibility; M.I.: Monolithic integration.

<sup>a</sup>Simulated values.

<sup>b</sup>Lowpass filters.

those of previous works. The filter of this work is advanced in the flexible design of polarization-rotated cavities free of geometrical distortion. It has evidenced great potentiality of the EWG and the ECR for 3-D-printing-compatible microwave waveguide devices. Waveguide filters with versatile transfer functions, improved stopband performance, and enhanced freedom of polarization orientations are to be developed as part of future work.

#### IV. CONCLUSION

A 3-D-printing-compatible design approach for polarization-rotated waveguide filters is proposed and it eliminates geometrical distortion occurred in the bending and twisting of conventional waveguide cavities. A new class of ECR-based BPF with a polarization rotation angle of 90° has been implemented monolithically by Polyjet additive manufacturing. The 3-D printed filter has successfully demonstrated excellent passband performance (RL: >20 dB; IL: ~0.4 dB;  $\Delta f$ : ~0.2%) and importance of the design approach.

#### ACKNOWLEDGMENT

This work was supported in part by the National Key Research and Development Program, China, under Subject No.2021YFA0715301, in part by the State Key Laboratory of Millimeter Waves, China, under Grant No.K202301, in part by the Guangdong Provincial Department of Science and Technology, China, under Project No.2020B1212030002, in part by the Shenzhen Science and Technology Innovation Commission, China, under Project No.QKTD20180412181337494 and Construction and Operation Project of Guangdong Provincial Key Laboratory and Guangdong-Hong Kong-Macau Joint Laboratory, and in part by the Postgraduate Education Branch of the China Education Society of Electronics.

#### REFERENCES

- M. A. Al-Tarifi and D. S. Filipovic, "Design and fabrication of a full W-band multi-step waveguide 90° twist," *IEEE Microw. Compon. Lett.*, vol. 26, no. 11, pp. 903–905, Nov. 2016.
- J.-Q. Ding, Y. Zhao, and S.-C. Shi, "A full WR-3 band and low-loss 90° waveguide twist based on CNC," *IEEE Trans. THz Sci. Techn.*, vol. 10, no. 1, pp. 93–96, Jan. 2019.
- A. A. Kirilenko, D. Y. Kulik, and L. A. Rud, "Compact 90° twist formed by a double-corner-cut square waveguide section," *IEEE Trans. Microw. Theory Techn.*, vol. 56, no. 7, pp. 1633–1637, Jul. 2008.
- S. Amari and M. Bekheit, "A new class of dual-mode dual-band waveguide filters," *IEEE Trans. Microw. Theory Techn.*, vol. 56, no. 8, pp. 1938–1944, Aug. 2008.
- Y. Xu, M. Sun, T.-H. Peng, Y. Luo, Y.-L. Pu, J.-X. Wang, Z.-W. Wu, G. Liu, and R. Yan, "Broadband and compact rectangular waveguide twist by using rigid waveguide," *Electron. Lett.*, vol. 54, no. 13, pp. 835–837, Jan. 2018.
- Y. Zhang, J. Xu, F. Zhang, X. He, X. Li, Y. Sun, and S. Xu, "A 3-D printed Ka-band twisted waveguide filter with filtering and polarization rotation," in *Proc. IEEE Int. Symp. Antennas Propag. USNC-URSI Radio Sci. Meeting*, Atlanta, GA, USA, Jul. 2019, pp. 1701–1702.
- Y. Zhang, F. Zhang, Y. Gao, J. Xu, C. Guo, and X. Shang, "3D printed waveguide step-twist with bandpass filtering functionality," *Electron. Lett.*, vol. 56, no. 11, pp. 527–528, May 2020.
- Q. Liu, Y. Zhang, F. Zhang, and J. Xu, "A 3D printed waveguide hybrid bandpass filter integrated with twisting and bending functionalities," in *Proc. IEEE Int. Symp. Antennas Propag. USNC-URSI Radio Sci. Meeting*, Denver, CO, USA, Jul. 2022, pp. 2000–2001.
- O. A. Peverini, M. Lumia, G. Addamo, F. Paonessa, G. Virone, R. Tascone, F. Calignano, G. Cattano, and D. Manfredi, "Integration of an H-plane bend, a twist, and a filter in Ku/K-band through additive manufacturing," *IEEE Trans. Microw. Theory Techn.*, vol. 66, no. 5, pp. 2210–2219, May 2018.
- J.-S. Hong and M. J. Lancaster, *Microstrip Filters for RF/Microwave Applications*. New York, NY, USA: Wiley, 2001.
- J. Shen and D. S. Ricketts, "Additive manufacturing of complex millimeter-wave waveguides structures using digital light processing," *IEEE Trans. Microw. Theory Techn.*, vol. 67, no. 3, pp. 883–895, Mar. 2019.
- J. Shen and D. S. Ricketts, "Compact W-band 'swan neck' turnstile junction orthomode transducer implemented by 3-D printing," *IEEE Trans. Microw. Theory Techn.*, vol. 68, no. 8, pp. 3408–3417, Aug. 2020.
- (May 2021). CST Studio Suite. Dassault Systèmes S.A. [Online]. Available: <https://www.3ds.com>.